

Current-controlled magnetization dynamics in the spin- $\uparrow$  transistor

Xuhui Wang and Gerrit E. W. Bauer

Kavli Institute of NanoScience, Delft University of Technology, 2628 C J Delft, The Netherlands

Teruo Ono

Institute for Chemical Research, Kyoto University, Uji Kyoto 611-0011, Japan

(Dated: October 28, 2021)

The current driven magnetization dynamics of a thin- $\text{In}$ , three magnetic terminal device (spin- $\uparrow$  transistor) is investigated theoretically. We consider a magnetization configuration in which all magnetizations are in the device plane, with source-drain magnetizations chosen fixed and antiparallel, whereas the third contact magnetization is allowed to move in a weak anisotropy field that guarantees thermal stability of the equilibrium structure at room temperature. We analyze the magnetization dynamics of the free layer under a dc source-drain bias current within the macrospin model and magneto-electronic circuit theory. A new tunable two-state behavior of the magnetization is found and the advantages of this phenomenon and potential applications are discussed.

## I. INTRODUCTION

The current induced magnetization excitation predicted by Slonczewski and Berger<sup>1,2</sup> has attracted considerable attention and the prediction of current-induced magnetization reversal has been confirmed by many experiments in nano-pillar structure consisting of two ferromagnetic layers with a high ("fixed") and a low ("free") coercivity, separated by a normal metal spacer.<sup>3,4,5,6</sup> Meanwhile, the investigations of charge and spin transport in thin- $\text{In}$  metallic conductors structured on a planar substrate have also been carried out.<sup>7,8,9,10,11,12</sup> The advantages of the planar structures are the flexible design and the relative ease to fabricate multi-terminal structures.<sup>13</sup> Recently, non-local magnetization switching in a lateral spin valve structure has been demonstrated.<sup>14</sup> In the present article we present a theoretical study on the dynamics of a lateral spin valve consisting of a normal metal  $\text{In}$  that is contacted by two magnetically hard ferromagnets. As sketched in Fig. 1, a slightly elliptic and magnetically soft ferromagnetic  $\text{In}$  is assumed deposited on top of the normal metal to form a spin- $\uparrow$  transistor.<sup>15</sup> The magnetization direction of the source-drain contacts lies antiparallel to each other in the plane of the magnetization of the third (free) layer. The configuration in which the source-drain contact magnetizations are oriented perpendicular to the plane is considered elsewhere.<sup>16</sup> A convenient and accurate tool to study the dynamic properties of our device is the magneto-electronic circuit theory (MECT) for charge and spin transport<sup>15</sup> combined with the Landau-Lifshitz-Gilbert equation in the macrospin model. The spin- $\uparrow$  scattering in normal and ferromagnetic metals and the spin-pumping effect are also taken into account.<sup>17,18</sup>

The article is organized as follows: In xII, we briefly review the MECT and Landau-Lifshitz-Gilbert equation for the macrospin model. In xIII, calculations of the spin transfer torque for our device are presented. xIV is devoted to the discussion of thermal (in)stability and in xV the magnetization dynamics is treated. The conclusions are summarized in xVI.

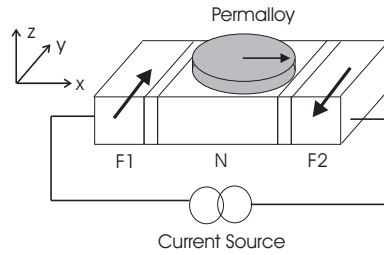


FIG. 1: The model system contains a normal metal sandwiched by two ferromagnetic leads and a circular soft ferromagnetic  $\text{In}$  (e.g., permalloy) on top of the normal metal. The magnetization unit vectors  $\mathbf{m}_1$ ,  $\mathbf{m}_2$ , and  $\mathbf{m}_3$  are initially aligned in the same, i.e.,  $xy$  plane.

## II. MAGNETO-ELECTRONIC CIRCUIT THEORY

We first consider a ferromagnet-normal metal (F/N) interface at quasi-equilibrium. The ferromagnet at a chemical potential  $\mu_0^F$  and spin accumulation  $\mu_s^F$  aligned along the magnetization direction. The chemical potential and spin accumulation in the normal metal are denoted by  $\mu_0^N$  and vector  $\mathbf{S}$ . The charge current  $I_c$  (in the unit of Ampere) and the spin current  $I_s$  (in the unit of Joule) entering the normal metal node are given by,<sup>15</sup>

$$\begin{aligned} I_c &= \frac{e}{2h} [2g(\mu_0^F - \mu_0^N) + pg_s^F - pg(\mathbf{S} \cdot \mathbf{m})] \\ I_s &= \frac{g}{8} [2p(\mu_0^F - \mu_0^N) + \mu_s^F - (1 - r)(\mathbf{S} \cdot \mathbf{m})]m \\ &\quad - \frac{rg}{8}\mathbf{S} - \frac{ig}{8}(\mathbf{S} \cdot \mathbf{m}) : \end{aligned} \quad (1)$$

From eq. (1) we may project out the component of  $I_s$  that is perpendicular to the magnetization direction and governs the spin transfer torque<sup>1,15</sup>

$$\mathbf{m} \cdot \mathbf{I}_s \cdot \mathbf{m} = \frac{rg}{8} [\mathbf{S} \cdot (\mathbf{S} \cdot \mathbf{m})\mathbf{m}] + \frac{ig}{8} (\mathbf{S} \cdot \mathbf{m}) : \quad (2)$$

In the above notations, the dimensionless total conductance  $g = g'' + g^\#$  and the mixing conductance are given by Landauer-Buttiker formulae, i.e.,

$$\begin{aligned} g''(\#) &= M \sum_{nm} T_{n(\#)}^{nm} T_{m(\#)}^{nm} ; \\ g^\# &= M \sum_{nm} r_n^{nm} (r_\#^{nm}) : \end{aligned} \quad (3)$$

where  $r_n^{nm}$  is the probability of a spin up (down) electron in mode  $m$  reflected into mode  $n$  in the normal metal and  $M$  is the total number of channels. The contact polarization is defined by  $p = (g'' - g^\#)/(g'' + g^\#)$ . The pumping current generated by the motion of the magnetization is<sup>17</sup>

$$I_s^{(p)} = \frac{hg}{8} r_m \frac{dm}{dt} + i \frac{dm}{dt} : \quad (4)$$

We consider the situation in which the dimension of the normal metal is smaller than the spin- $\uparrow\downarrow$  length, so that the spin accumulation does not vary spatially in the node.

$$I_s^{(f)} = \frac{g_f}{4} \mathbf{S} \quad (5)$$

where  $g_f = h \rho_{DOS} V_N = \frac{N}{\tau_f}$ ,  $\rho_{DOS}$  and  $V_N$  are the density of states of the electrons and the volume of the normal metal,  $\tau_f$  is the spin- $\uparrow\downarrow$  relaxation time in the normal metal node. The charge and spin currents entering the normal metal obey the conservation laws

$$\begin{aligned} \sum_i I_{c;i} &= 0 ; \\ \sum_i I_{s;i} + I_{s;i}^{(p)} &= I_s^{(f)} : \end{aligned} \quad (6)$$

## III. SPIN TRANSFER TORQUE

In the structure depicted in Fig. 1, the source-drain magnetizations are aligned anti-parallel along the  $y$ -axis in order to inject a large spin accumulation into  $N$ , i.e.,  $\mathbf{m}_1 = (0; +1; 0)$  and  $\mathbf{m}_2 = (0; -1; 0)$ . Connecting the ferromagnets to reservoirs and applying a bias current  $I_0$  via the two ferromagnetic leads, the conservation of charge current dictates that  $I_{c;1} = I_0$  and  $I_{c;2} = -I_0$  at the F1/N and F2/N interfaces, which gives

$$\mu_0^1 - \mu_0^N = (\mu_0^2 - \mu_0^N) = \frac{I_0 h}{ge} + \frac{1}{2} p S_y : \quad (7)$$

The free layer is electrically floating, hence there is no net charge current flowing through F3N interface,  $I_{c;3} = 0$ . The spin accumulation in the free layer  $F_s = \mu_F - \mu_N$ , directed along magnetization  $m_3$ , is governed by the spin diffusion equation,<sup>19</sup>

$$\frac{\partial^2 F_s(z)}{\partial z^2} = -\frac{F_s(z)}{l_{sd}^2} \quad (8)$$

which satisfies the following boundary conditions. At the interface the continuity of longitudinal spin current dictates

$$-\frac{\partial \mu_F}{\partial z} \Big|_{z=0} = \frac{\partial \mu_N}{\partial z} \Big|_{z=0} = \frac{2e^2}{hA} I_{s;3} \quad (9)$$

and the vanishing spin current at the end of the ferromagnet implies

$$-\frac{\partial \mu_F}{\partial z} \Big|_{z=d} = \frac{\partial \mu_N}{\partial z} \Big|_{z=d} = 0 \quad (10)$$

The solution of eq. (8) reads

$$F_s(z) = \frac{h}{3 + \tilde{\gamma} \tanh(\frac{d}{l_{sd}})} \frac{\cosh(\frac{z-d}{l_{sd}}) m_3 \cdot S}{\cosh(\frac{d}{l_{sd}})} \quad (11)$$

where  $\gamma_3 = g_3(1 - \beta_3^2)/8$  characterizes the contact F3N and  $\tilde{\gamma} = hA \mu_F \mu_N = (e^2 l_{sd} / (g_F + g_N))$  describes the bulk properties of the free layer with arbitrary  $m_3$ . The conservation of spin currents in eq. (6) generates three linear equations that determine the spin accumulation  $S$  in the normal metal as

$$S = \hat{\gamma}(g; g_3) \gamma_3 I_s^{(p)} + W_b \quad (12)$$

where the vector  $W_b = (0; 2\hbar p I_0/e; 0)$  is the contribution from the bias current and the elements of the symmetric matrix  $\hat{\gamma}(g; g_3)$  is listed in the Appendix. Equation (2) determines the spin transfer torque acting on the free layer magnetization, which can be arranged as

$$L = \frac{3\gamma_3}{8} \hat{\gamma}(g; g_3) \gamma_3 I_s^{(p)} + W_b \quad (13)$$

and the components of the matrix  $\hat{\gamma}(g; g_3)$  are listed in the Appendix.

#### IV. THERMAL STABILITY

The spin transfer torque rotates the magnetization out of the equilibrium hence increasing the magnetostatic energy  $E_{MS}$ . The initial magnetization is stable against thermal fluctuations when

$$E_{MS} > k_B T; \quad (14)$$

where  $k_B$  is the Boltzmann constant and  $T$  the temperature. For an elliptic perm alloy film, disregarding any residual crystalline anisotropy, the effective field due to the shape anisotropy can be written as

$$H_e = -\frac{1}{2} M_s (N_x m_x^2 + N_y m_y^2 + N_z m_z^2); \quad (15)$$

introducing the saturation magnetization  $M_s$  and demagnetizing factors  $N_x, N_y$  and  $N_z$ .<sup>20</sup> When the magnetization is slightly out of plane, the difference between the magnetostatic energy for magnetizations along the hard-axis and easy-axis reads  $E_{MS} = \frac{1}{2} M_s^2 (N_y - N_x) = 2$ . For a very flat ellipsoid (the thickness is much smaller than the lateral dimensions) and slight ellipticity (large aspect ratio  $\gg 1$ ), we can expand the demagnetizing factors at  $\epsilon = 1$  such that

$$N_y - N_x = \frac{d}{4a} \frac{(\epsilon^2 + 4\epsilon + 1)(1 - \epsilon^2)}{(\epsilon^2 + 1)^2}; \quad (16)$$

where  $a, b$  and  $d$  are the lengths of easy-axis, hard axis and the thickness of the perm alloy film. The aspect ratio is defined as  $\gamma = b/a$ . The requirement  $E_{MS} > k_B T$  gives

$$\frac{(\gamma^2 + 4\gamma + 1)(1 + \gamma^2)}{(1 + \gamma^2)^2} > \frac{8k_B T}{\mu_0 M_s^2 \gamma^2 a d^2} : \quad (17)$$

The saturation magnetization of perm alloy is  $M_s = 8 \times 10^6 \text{ A m}^{-1}$ . For thickness  $d = 5 \text{ nm}$  and easy axis  $a = 200 \text{ nm}$ , the right hand side of eq. (17) is at room temperature approximately  $= 8.36 \times 10^3$  and therefore stability requires that

$$1 > \frac{2}{3} \gamma ; \quad (18)$$

which suggests that even for almost circular perm alloy discs, e.g.,  $\gamma = 0.9$ , thermal fluctuations around the equilibrium configuration are small.

## V. MAGNETIZATION DYNAMICS

Here we focus on the free layer magnetization dynamics in the macrospin model. The Landau-Lifshitz-Gilbert (LLG) equation modified by the spin transfer torque [eq. (13)] reads

$$\frac{1}{\gamma} \frac{dm}{dt} = -\gamma m \times H_e + \frac{\gamma_0}{\gamma} m \times \frac{dm}{dt} + \frac{1}{\gamma M_s} L : \quad (19)$$

Included in the torque term, i.e., Eq. (13), an expression

$$\hat{\Gamma}^0 = \frac{\hbar^2 g_3^2}{8 \gamma M_s} \hat{g}(\mathbf{g}; \mathbf{g}) \quad (20)$$

appears as an enhancement of the Gilbert damping,<sup>17</sup> which depends on the direction of the magnetization and shows tensor property of the pumping induced damping enhancement.<sup>21</sup> When the conductance at the F3N contact is much larger than the source-drain contacts and the spin flip in the normal metal is negligible, i.e.,  $g_3 \gg g$  and  $g_3 \gg g_{sf}$ , the tensor  $\hat{\Gamma}^0$  converges to<sup>21</sup>

$$\frac{\hbar R e g_3^{\#}}{4 \gamma M_s} @ \begin{pmatrix} 1 & m_x^2 & m_x m_y & m_x m_z \\ m_x m_y & 1 & m_y^2 & m_y m_z \\ m_x m_z & m_y m_z & 1 & m_z^2 \end{pmatrix} A ; \quad (21)$$

which in the LLG equation reduces to a diagonal matrix

$$\hat{\Gamma}^0 = \frac{\hbar R e g_3^{\#}}{4 \gamma M_s} \hat{1} \quad (22)$$

and the coefficient in front of the matrix is exactly the value derived for the single F3N junction<sup>17</sup>. In the same limit, the bias-driven term of the torque reads,

$$\frac{1}{\gamma M_s} L_b = \frac{\hbar p I_0}{2 \gamma M_s e j} @ \begin{pmatrix} 0 & 1 \\ 1 & m_x m_y \\ m_x m_y & 1 \\ m_y m_z & m_z^2 \end{pmatrix} A : \quad (23)$$

In the following discussions, we denote the enhanced Gilbert damping parameter as  $\gamma = \gamma_0 + \gamma^0$ , where  $\gamma^0$  is the diagonal entry in eq.(22). The LLG equation then reads

$$\frac{1}{\gamma} \frac{dm}{dt} = -\gamma m \times H_e + \frac{\gamma_0}{\gamma} m \times \frac{dm}{dt} + \frac{1}{\gamma M_s} L_b : \quad (24)$$

For ultrathin perm alloy films, without external field and crystalline anisotropy, the magnetization is confined in the plane by the shape anisotropy field given by eq. (15). Equation (24) is a nonlinear differential equation that can be reformulated as

$$\frac{dm}{dt} = f(m; I_0) \quad (25)$$

where  $f(\mathbf{m}; I_0)$  is a vector function of magnetization  $\mathbf{m}$  and bias current  $I_0$ . According to the theory of differential equations<sup>22</sup>, we find two "equilibrium points" at which  $d\mathbf{m}/dt$  vanishes  $\mathbf{m}_1 = (1; 0; \hbar p I_0 / [2e_0 V M_s^2 (N_z - N_x)])$  and  $\mathbf{m}_2 = (0; 1; 0)$ . Expanding eq. (24) at point  $\mathbf{m}_2$  and keeping only the first-order derivatives with respect to the magnetization, i.e.,

$$\frac{d\mathbf{m}}{dt} = \frac{\partial f}{\partial \mathbf{m}} \Big|_{\mathbf{m}_2}; \quad (26)$$

where  $\partial f / \partial \mathbf{m}$  is a matrix with elements given by  $\partial f_i / \partial m_j$ . Equation (26) has non-zero solution when

$$\det \frac{\partial f}{\partial \mathbf{m}} \Big|_{\mathbf{m}_2} = 0; \quad (27)$$

This determines the critical current that is necessary to obtain the maximum in-plane rotation, i.e.,  $\theta = 2$ :

$$I_c = \frac{2e_0 V M_s^2 P}{\hbar p} \frac{(N_z - N_y)(N_y - N_x)}{(N_z - N_x)} \quad (28)$$

The LLG equation augmented by the spin transfer torque for the present configuration suggests a two-state behavior of the magnetization: Below the critical current  $I_c$ , the magnetization is pushed out of the initial position (easy axis), then undergoing damped precessions and finally stops along the easy axis but with a small z-component, i.e., the equilibrium given by  $\mathbf{m}_1$ . At that position, the demagnetizing field is balanced by the spin torque. Above the critical current, the magnetization precesses out of the easy axis and rotates to the hard axis without any precession.

We simulate the magnetization dynamics for a polarization  $p = 0.4$  of the F3JN and a real part of the mixing conductance  $\text{Re} g_3^{\text{F3JN}} A^{-1} = 4.1 \times 10^{15} \text{ cm}^2$ .<sup>23</sup> The long semiaxis, short semiaxis and the thickness of the permalloy island are  $a = 200 \text{ nm}$ ,  $b = 190 \text{ nm}$ , and  $d = 5 \text{ nm}$ , respectively. The calculated demagnetizing factors are  $N_y = 0.0224$  and  $N_x = 0.0191$ .<sup>20</sup> The single-spin density of states in the normal metal is  $D_{\text{DOS}} = 2.4 \times 10^{28} \text{ eV}^{-1} \text{ m}^{-3}$ .<sup>9</sup> The bulk value of the Gilbert damping parameter is  $\alpha_0 = 0.006$  and the calculated enhancement of Gilbert damping is  $\alpha = 0.015$ .<sup>17</sup> According to eq. (28), for the above dimensions, the critical current to achieve  $\theta = 2$  is  $I_c = 139 \text{ mA}$ , which agrees well with the numerical results. Below the critical current, e.g.,  $I_0 = 30 \text{ mA}$ , the equilibrium z-component determined by the expression of  $\mathbf{m}_1$  is 0.0087, which also agrees with the numerical results shown in Fig. 4. The trajectory of the magnetization when suddenly switching on the bias current  $I_0 = 30 \text{ mA}$  is depicted in Fig. 2. The magnetization starts from the easy axis (point I in the figure), undergoes a damped oscillation and finally stops at point F, where the spin transfer torque induced by the spin accumulation in the normal metal is balanced by the torque generated by the anisotropy field. Fig. 7 shows the trajectory of the magnetization under switching on a the bias current  $I_0 = 160 \text{ mA}$ , which is above the critical current. Figures 5 and 6 are the time dependence of the y and z-components of the free layer magnetization. These figures indicate that the magnetization response to a large current is close to a step function. A smaller size of the permalloy film requires a smaller critical current, as indicated by eq. (28). In the above simulation, we did not take into account the effect of a finite RC time for switching on the bias current. A longer rising time of the bias current implies that it takes longer before the magnetization reaches the steady state position. But the magnitude of the critical current does not depend on how the bias current transient.

We finally note that with the dimensions chosen here, the bias currents generate a significant in-plane rsted field that may interfere with the spin-torque effect. It can be avoided, e.g., by spatially separating the free layer from the current path (but within the spin-diffusion)<sup>14</sup> or by generating a neutralizing rsted field by a neighboring circuit (suggested by Siegmann).

The advantage of the proposed device mainly comes from the two-state behavior separated by the critical current, which can be utilized as the 0 and 1 states in current controlled memory elements. We notice that after the magnetization being switched to the hard axis, only small current is needed to maintain the position stable against thermal fluctuations. Another possible application could be the implementation of such device into spin-torque transistors<sup>13</sup> to achieve the gain of current since the angle of the magnetization in the above device is tunable by the bias. The magnetization can be also used as a spin battery that is "charged" in the high energy state (hard axis) and relaxes a spin current into the normal metal when relaxing to the ground state (easy axis). The induced spin accumulation then creates voltage difference over the source and drain contacts.

## VI. CONCLUSIONS

In this article, the magnetization dynamics of a spin-dip transistor has been studied in the macrospin LLG equation combined with MECT. We found a two-state behavior of the free layer magnetization controlled by the current

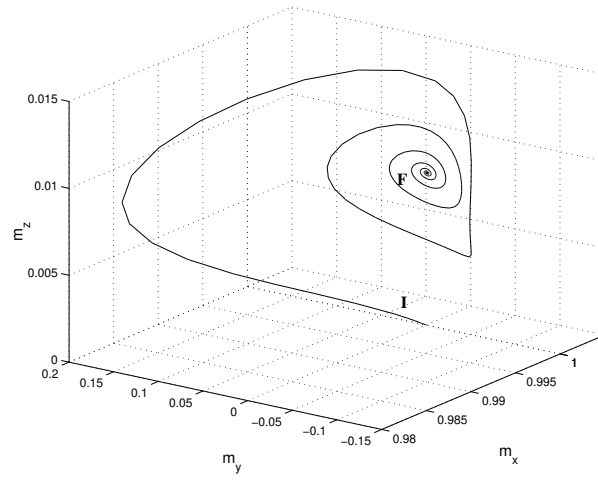


FIG . 2: The trajectory of the magnetization with the bias current  $I_0 = 30$  mA, which is below the critical current. The magnetization initially aligned along easy axis (x-axis) and after the damped oscillation it stops along the easy axis with small out-of-plane component.

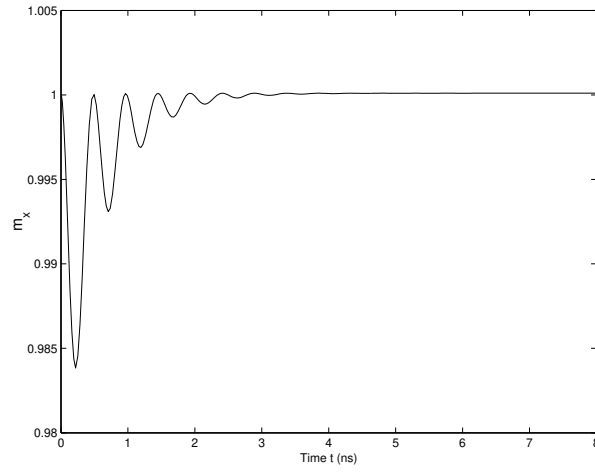


FIG . 3: The x-component of the magnetization vs time (in ns). The bias current is 30 mA.

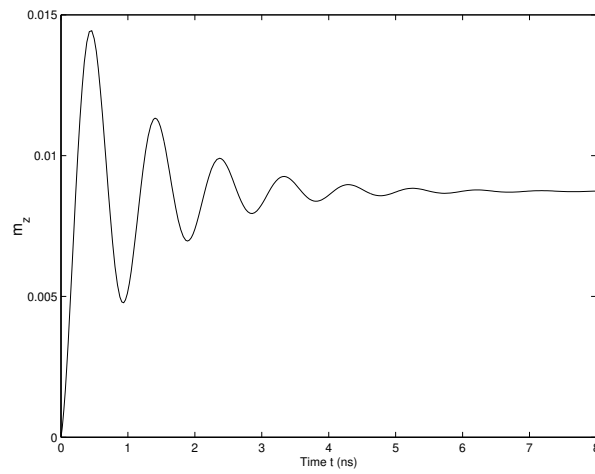


FIG . 4: The z-component of the magnetization vs time (in ns). The bias current is 30 mA.

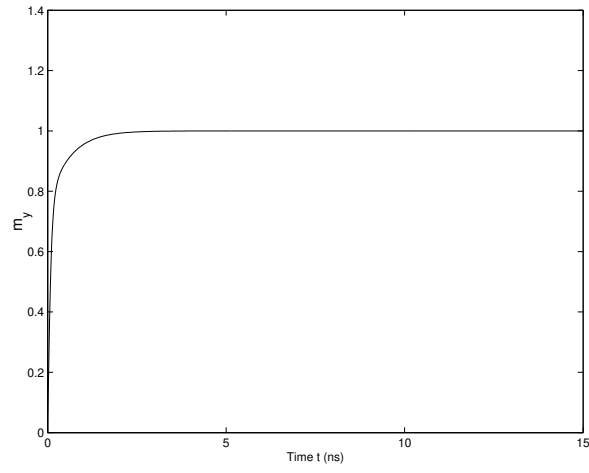


FIG . 5: The y-component of the magnetization vs time. The bias current is 160 mA, which is above the critical current.

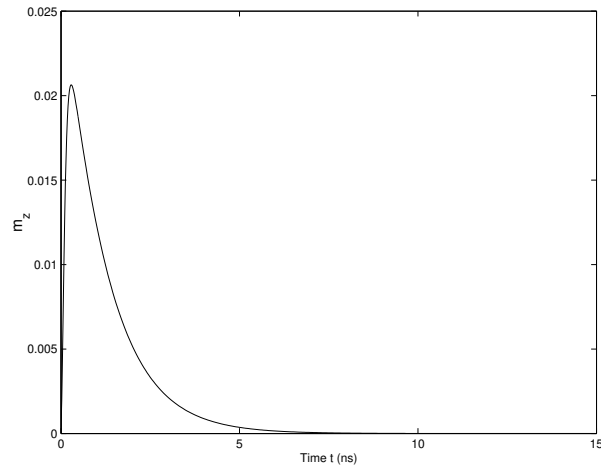


FIG . 6: The z-component of the magnetization vs time, with bias current 160 mA that is above the critical current.

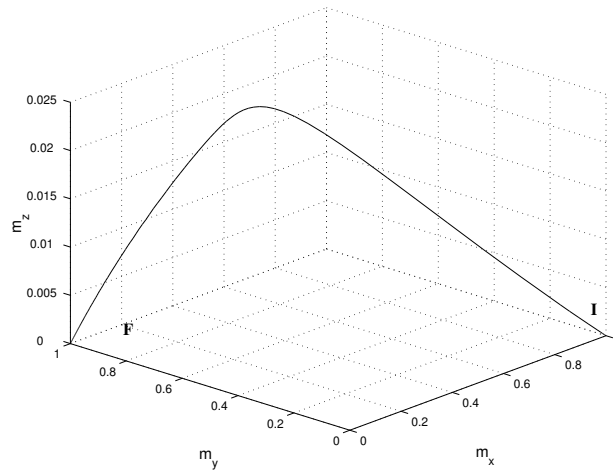


FIG . 7: The trajectory of the magnetization under the bias above the critical current,  $I_0 = 160$  mA. The magnetization initially aligned along easy axis (point I).

induced spin transfer torque and spin pumping. The two regimes are separated by a critical current, below which the magnetization undergoes a damped oscillation and stops along the easy axis with small z-component. Above the critical current, the magnetization rotates to the hard (y-) axis without precession. The critical current is found to depend on the size of the free layer, the aspect ratio of the ellipsoid, and the source-drain contact polarizations. The thermal instability analysis indicates that at room temperature the predicted effects are visible even for very large aspect ratios.

#### Acknowledgments

We thank J.C. Slonczewski and A. Kovalev for discussions. X. Wang thanks H. Saarikoski for his help on MatLab. This work is supported by NanoNed and FOM.

- 
- <sup>1</sup> J.C. Slonczewski, J. Magn. Magn. Mater. 159, L1 (1996).
  - <sup>2</sup> L. Berger, Phys. Rev. B 54, 9359 (1996).
  - <sup>3</sup> J.A. Katine, F.J. Albert, R.A. Buhrman, E.R. Myers, and D.C. Ralph, Phys. Rev. Lett. 84, 3149 (2000).
  - <sup>4</sup> E.B. Myers, F.J. Albert, J.C. Sankey, E. Bonet, R.A. Buhrman, and D.C. Ralph, Phys. Rev. Lett. 89, 195801 (2000).
  - <sup>5</sup> S.I. Kiselev, J.C. Sankey, I.N. Krivorotov, N.C. Emley, R.J. Schoelkopf, R.A. Buhrman, and D.C. Ralph, Nature (London) 425, 380 (2003).
  - <sup>6</sup> W.H. Rippard, M.R. Pufall, S. Kaka, S.E. Russek, and T.J. Silva, Phys. Rev. Lett. 92, 027201 (2004).
  - <sup>7</sup> F.J. Jedema, A.T. Filip, and B.J. van Wees, Nature 410, 345 (2001).
  - <sup>8</sup> F.J. Jedema, H.B. Heersche, A.T. Filip, J.J.A. Baselmans, and B.J. van Wees, Nature 416, 713 (2002).
  - <sup>9</sup> M. Zolnariu and B.J. van Wees, Phys. Rev. Lett. 91, 186601 (2003).
  - <sup>10</sup> T. Kimura, J. Hamrle, Y. Otani, K. Tsukagoshi, and A. Aoyagi, App. Phys. Lett. 85, 3501 (2004).
  - <sup>11</sup> S.O. Valenzuela and M. Tinkham, App. Phys. Lett. 85, 5914 (2004).
  - <sup>12</sup> Y. Ji, A. Homann, J.S. Jiang, and S.D. Bader, App. Phys. Lett. 85, 6218 (2004).
  - <sup>13</sup> G.E.W. Bauer, A. Bataas, Y. Tserkovnyak, and B.J. van Wees, App. Phys. Lett. 82, 3928 (2003).
  - <sup>14</sup> T. Kimura, Y. Otani, and J. Hamrle, cond-mat/0508559 (2005).
  - <sup>15</sup> A. Bataas, Y.V. Nazarov, and G.E.W. Bauer, Phys. Rev. Lett. 84, 2481 (2000).
  - <sup>16</sup> X. Wang, G.E.W. Bauer, and A. Homann, cond-mat/0601630 (2006).
  - <sup>17</sup> Y. Tserkovnyak, A. Bataas, and G.E.W. Bauer, Phys. Rev. Lett. 88, 117601 (2002).
  - <sup>18</sup> Y. Tserkovnyak, A. Bataas, G.E.W. Bauer, and B.I. Halperin, Rev. Mod. Phys. 77 (2005).
  - <sup>19</sup> M. Johnson and R.H. Silsbee, Phys. Rev. B 37, 5312 (1988).
  - <sup>20</sup> J. A. Osborn, Phys. Rev. 67, 351 (1945).
  - <sup>21</sup> X. Wang, G.E.W. Bauer, Y. Tserkovnyak, and A. Bataas, unpublished (2005).
  - <sup>22</sup> L. Perko, Differential Equations and Dynamical Systems (Springer, Berlin, 1996), 2nd ed.
  - <sup>23</sup> K. Xia, P.J. Kelly, G.E.W. Bauer, A. Bataas, and I. Turek, Phys. Rev. B 65, 220401 (2002).

#### APPENDIX A: SPIN ACCUMULATION AND SPIN TRANSFER TORQUE

The elements of the symmetric matrix  $\hat{g}(g_3)$  in eq. (12) are listed in the following

$$g_{11} = [g_3 g_3 + 2g_{sf} + 2(1 - \beta^2)g] \mathcal{L} g + g_3 g_3 + 2g_{sf} \quad \mathcal{G} (g_3 - (1 - \beta^2)(1 - g_3)) m_z^2 = G \quad (A 1)$$

$$(2 g + g_3 g_3 + 2g_{sf}) g_3 [g_3 - (1 - \beta^2)(1 - g_3)] m_y^2 = G$$

$$g_{12} = g_{21} = (2 g + g_3 g_3 + 2g_{sf}) g_3 [g_3 - (1 - \beta^2)(1 - g_3)] m_x m_y = G \quad (A 2)$$

$$g_{13} = g_{31} = [g_3 g_3 + 2g_{sf} + 2(1 - \beta^2)g] g_3 [g_3 - (1 - \beta^2)(1 - g_3)] m_x m_z = G \quad (A 3)$$

$$g_{22} = (2 g + g_3 g_3 + 2g_{sf}) \mathcal{L} g + g_3 g_3 + 2g_{sf} \quad \mathcal{G} (g_3 - (1 - \beta^2)(1 - g_3)) (m_x^2 + m_z^2) = G \quad (A 4)$$

$$g_{23} = g_{32} = (2 g + g_3 g_3 + 2g_{sf}) g_3 [g_3 - (1 - \beta^2)(1 - g_3)] m_y m_z = G \quad (A 5)$$

$$g_{33} = [g_3 g_3 + 2g_{sf} + 2(1 - \beta^2)g] \mathcal{L} g + g_3 g_3 + 2g_{sf} \quad \mathcal{G} (g_3 - (1 - \beta^2)(1 - g_3)) m_x^2 = G \quad (A 6)$$

$$(2 g + g_3 g_3 + 2g_{sf}) g_3 [g_3 - (1 - \beta^2)(1 - g_3)] m_y^2 = G$$

where we have introduced the following notation

$$G = (2g + g_3 + 2g_{sf}) [(g_3 + 2g - 2p^2g + 2g_{sf})(2g + 2g_{sf} + (1 - p^2)(1 - g_3)g_3) + 2(p^2 - 1 + g)(g_3 - (1 - p^2)(1 - g_3))g_3m_y^2]; \quad (A 7)$$

and

$$g_3 = \frac{g_3}{g_3 + \sim \tanh(d=l_{sd})} : \quad (A 8)$$

The matrix contained in the expression of spin transfer torque eq. (13) has the following components

$$_{11} = [(g_3 + 2g_{sf} + 2(1 - p^2)g)(2g + g_3 + 2g_{sf} - g_3(g_3 - (1 - p^2)(1 - g_3))m_z^2) - G(2g + g_3 + 2g_{sf})[(g_3 - (1 - p^2)(1 - g_3))g_3m_y^2 + (g_3 + 2g_{sf} + 2(1 - p^2)g)m_x^2)] = G \quad (A 9)$$

$$_{12} = (2g + g_3 + 2g_{sf})(2g + 2g_{sf} + (1 - p^2)(1 - g_3)g_3)m_xm_y = G \quad (A 10)$$

$$_{13} = [(g_3 + 2g_{sf} + 2(1 - p^2)g)(2g + 2g_{sf} + (1 - p^2)(1 - g_3)g_3)m_xm_z = G \quad (A 11)$$

$$_{21} = (2g + g_3 + 2g_{sf})(2g_{sf} + 2(1 - p^2)g + (1 - p^2)(1 - g_3)g_3)m_xm_y = G \quad (A 12)$$

$$_{22} = (2g + g_3 + 2g_{sf})(2g + 2g_{sf} + (1 - p^2)(1 - g_3)g_3)(1 - m_y^2) = G \quad (A 13)$$

$$_{23} = (2g + g_3 + 2g_{sf})(2g_{sf} + 2(1 - p^2)g + (1 - p^2)(1 - g_3)g_3)m_y m_z = G \quad (A 14)$$

$$_{31} = [(g_3 + 2g_{sf} + 2(1 - p^2)g)(2g + 2g_{sf} + (1 - p^2)(1 - g_3)g_3)m_xm_z = G \quad (A 15)$$

$$_{32} = (2g + g_3 + 2g_{sf})(2g + 2g_{sf} + (1 - p^2)(1 - g_3)g_3)m_y m_z = G \quad (A 16)$$

$$_{33} = [(g_3 + 2g_{sf} + 2(1 - p^2)g)(2g + g_3 + 2g_{sf} - g_3(g_3 - (1 - p^2)(1 - g_3))m_x^2) - G(2g + g_3 + 2g_{sf})[(g_3 - (1 - p^2)(1 - g_3))g_3m_y^2 + (g_3 + 2g_{sf} + 2(1 - p^2)g)m_z^2)] = G : \quad (A 17)$$